

Optical properties comparison between similar thickness

TiO₂ polymorphs

Cameron Stewart

An undergraduate thesis advised by Dr. Janet Tate

submitted to the Department of Physics, Oregon State University

in partial fulfillment of the requirements of the degree BSc in Physics

Submitted on May 22, 2020

List of Figures

2.1	TiO ₂ Polymorphs	6
2.2	Diffraction Grating Example	8
2.3	Bandgap for semiconductors	9
2.4	EM wave interaction with thin film	10
3.1	Grating Spectrometer setup	11
3.2	Optical setup for T and R measurements	12
3.3	Tauc analysis	14
4.1	Sample TiO ₂ _86_Pre T and R	18
4.2	SiO ₂ T and R	19
4.3	$\frac{T}{1-R}$ pre anneal curves	20
4.4	$\frac{T}{1-R}$ post anneal curves	21
4.5	Absorption coefficients pre anneal thin films	22
4.6	Absorption coefficients post anneal thin films	23
4.7	TiO ₂ pure phase polymorph $\frac{T}{(1-R)}$	24
6.1	Ellipsometer and spectrometer thickness comparison	31
6.2	Ellipsometer and spectrometer thickness comparison	32

Contents

1 Abstract	4
2 Introduction	5
2.1 Goal	5
2.2 Optical Properties of Thin Films	5
2.2.1 Refractive Index and Transmission and Reflection	6
2.2.2 The Bandgap	9
2.3 Interference Fringes: Destructive and Constructive Waves	9
3 Materials and Methods	11
3.1 Grating Spectrometer	11
3.2 Error due to alignment	12
3.3 Index Calc	13
3.4 Tauc Analysis	13
3.5 O ₂ deficiency	14
4 Results and Discussion	16
4.1 Transmission and Reflection	17
4.2 Absorption Coefficient	21
4.3 Pure Phase Films	23
4.4 Band Gap Analysis	24
5 Conclusion	28
6 Appendix	31
6.1 Section 1: Ellipsometer vs Spectrometer Comparison	31

1 Abstract

The optical properties of titanium dioxide(TiO_2) thin films vary on if the oxide is in an amorphous or crystalline state as well as the thickness of each film. Amorphous TiO_2 can be transformed through annealing into three distinct polymorphs: rutile, brookite, anatase. With recent developments, parameters can be set for the deposition process so that the amorphous precursors can be made where the crystalline phases are known. To determine these optical properties, transmission and reflection spectroscopy was performed over the wavelength range 200 nm to 1000 nm.

Previous research had shown that absorption observed in the longer wavelength range ($> 600\text{nm}$) was strong for brookite and rutile thin films. This was observed for TiO_2 films of very different thicknesses and different phase combinations. This paper expands upon these findings by exploring pure phase TiO_2 thin films with similar thicknesses. The absorption coefficients for the polymorphs are determined in part by the thickness. Similar thickness films will remove any dependency when comparing these coefficients for different polymorph phases. The same observance of absorbance in the long wavelengths was found in the pure phase films. Anatase absorbed very little with brookite absorbing more and rutile absorbing the most out of the three polymorphs. This follows the reasoning that defect states found in the amorphous precursors are present with films of similar thickness and pure phase.

Performing a Tauc analysis approximated the bandgap energies for these films. The Tauc analysis indicates on average the bandgap energy for anatase and brookite films decreases after the annealing process. The indirect bandgaps for the same polymorphs however, on average retained the same bandgap energy when transitioning from pre to post anneal. The single rutile pure phase thin film also presented a similar behavior for the bandgap energy for the direct and indirect.

2 Introduction

2.1 Goal

Titanium Dioxide(TiO_2) has been a widely studied in the material science community[1]. The applications vary from having self cleaning properties to being hydrophilic when exposed to UV light and hydrophobic in a light deprived environment[2]. To make the oxide viable for commercial use, the band gap, index of refraction and the allotropic forms must be fleshed out in understanding of how they work. Depositing TiO_2 onto a substrate allows for easy analysis through either electrical or optical methods. Creating thin films of similar thicknesses and atomic orientation is very difficult. Dr. Janet Tate's research group, the Tate Lab have been working to determine a effective method for producing these TiO_2 where we can predict the amorphous precursor's for thin films before annealing them. The method used by Okan Agirseven in the Tate lab for producing these thin films is RF sputtering currently[3]. Recently he has managed to determine parameters to set where the amorphous precursors can have their polymorph phases known after annealing. This has allowed him to produce films of similar thicknesses made up of 100% of each allotropic form of TiO_2 . Patrick Berry performed transmission(T) and reflection(R) measurements for films with some pure phase however these films were of different thicknesses[4]. The goal of this project was to determine how the optical properties vary across the allotropic forms when now being able to produce them at the same thickness.

2.2 Optical Properties of Thin Films

RF Sputtering allow molecules to be deposited onto a substrate surface uniformly[6]. This uniform deposition ensures testing at any position along the materials surface provides similar results. TiO_2 is a oxide semiconductor that can be deposited with this technique, onto silica (SiO_2) substrates. When deposited onto silica, the TiO_2 's molecular structure has long-range disorders. This is known as the amorphous form of TiO_2 . Rearranging this state requires annealing the molecular structure reforming the TiO_2 into a crystalline state in any variation of three polymorphs. These polymorphs include brookite, rutile, and anatase as seen in figure 2.1 . Each one is made up of the molecule TiO_2 however their geometric arrangement of Ti and O_2 will vary. Due to this chemical variance, the three polymorphs, bandgap, transmission of light, reflection of light, and index of refraction will also differ.

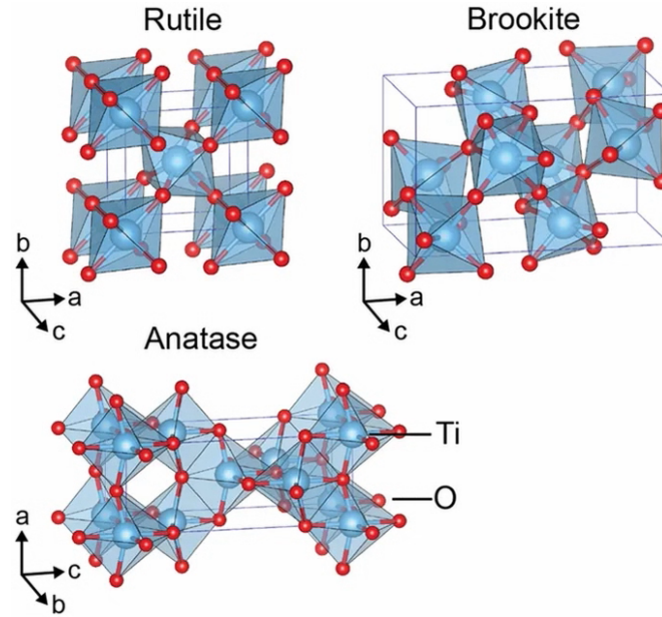


Figure 2.1: Graphical interpretation of the TiO_2 polymorphs brookite, rutile, and anatase. The red dots indicate the oxygen atoms surrounding Ti atoms arranged as a crystalline structure .[5]

RF Sputtering is a effective method for creating TiO_2 made up of a smooth layer with a combination of any of the three polymorphs. The issue that has arisen is the amorphous precursors of TiO_2 can be made up of any random combination of brookite, rutile and anatase. The inability to make a thin films with predetermined specifications prevents efficient analysis of TiO_2 . With recent developments from Okan Agirseven's research, these amorphous precursors can have their phases determinable once they have crystallized. Since each polymorph possesses different optical properties, creating parameters so for example a thin film made of 100% of anatase, would provide easy examination of how the bandgap changes for a thin film of 100% of brookite or 100% rutile.

2.2.1 Refractive Index and Transmission and Reflection

All electromagnetic radiation propagates through a vacuum at the speed of light. As light approaches a medium other than a vacuum, the speed decreases. This change in speed is classified by the refractive index, a ratio which takes the quotient of the speed of light in a vacuum divided by the speed in a different medium.

$$c = \frac{n}{v}, \quad (1)$$

c is speed of light = $3 \times 10^8 \frac{m}{s}$ and v is the speed of light through a medium. The value for n in is the real component of the refractive index which is accompanied by an imaginary component κ . Therefore, the complex refractive index is,

$$n = n_{real} + i\kappa, \quad (2)$$

The imaginary component κ is the extinction coefficient which accounts for the attenuation as the light travels through a new medium. An attenuation in optics is the gradual loss of intensity which light experiences. This attenuation includes the scattering of light and the absorption from the medium the light travels through. TiO_2 for example contains an absorption between the wavelengths of 300 nm to 400 nm. This absorption is known as the bandgap which will be further discussed in a later section. The drop of the flux density occurs as a rate of e^{-1} , where the wave travels the distance y

$$y = \frac{1}{\alpha}, \quad (3)$$

which is the penetration depth within the material[7]. For TiO_2 , this distance is big enough that the material can be transparent as its thickness is much less in terms of length. To calculate the real part of the index of refraction, an equation known as the Sellmeier equation can be used to determine the n value

$$n^2(\lambda) = 1 + \sum_i \frac{B_i \lambda^2}{\lambda^2 - C_i}, \quad (4)$$

where B_i and C_i are values that must be experimentally determined with varying λ (wavelength) values.

The imaginary component can be found from

$$\kappa = \frac{\alpha \lambda}{4\pi}, \quad (5)$$

where α is the absorption coefficient. Looking at the behavior of light interacting with a medium other than a vacuum, there is absorption as well as the transmission of light and reflection. The transmission of light is the amount of radiation that propagates through the medium and exits outside of the opposing side. TiO_2 visually is transparent for thin films which allows a large portion of the light to transmit

through. The rest of the light must get reflection after the incident light interacts with the medium. Combining the absorption, transmission, and reflection should equal the flux before the light interacted with the medium. T and R spectroscopy is a direct way that the transmission and reflection can be measured.

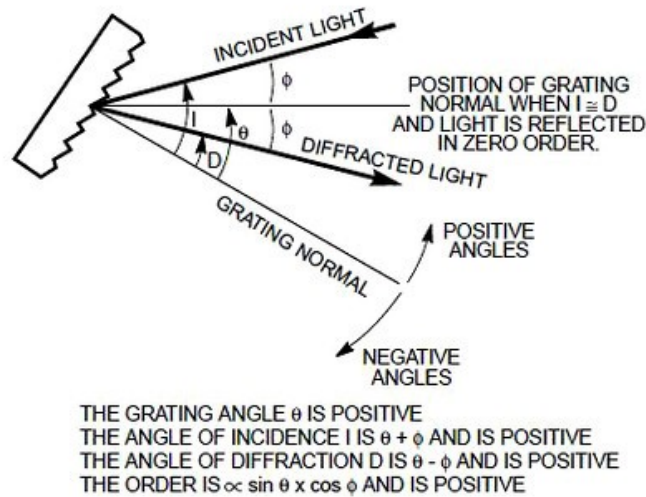


Figure 2.2: Example of a reflective grating where the angle of incident approaches at some angle. Depending on this θ_i , the wavelength of light will be dependant on that incident angle with respect to the grating [8]

Using diffraction grating, in figure 2.2, the incident light approaches the grating then once the two interact, the light gets emitted back out into the medium. The angle the light hits the grating will determine the wavelength of light that gets emitted. For this project, by using this technique the wavelength of light can be generated across a range of wavelengths. The incident light is made up of the T and R

$$I = T + R + A, \quad (6)$$

where A is the absorption. This reflection and transmission data can then be plugged into a formula confirmed by

$$\frac{T}{(1 - R)} = e^{-\alpha d}, \quad (7)$$

determining the α (absorption coefficient) and d (width of material) becomes doable once these transmission and reflection values are found[9].

2.2.2 The Bandgap

The bandgap is the distance between the valence and conduction band for a material. The bandgap must be small enough that the electrons can transition from the valence band to the conduction band[11]. The valence band is the region where the electrons would be and when the energy needed to leap to the conduction band is met, the empty “holes” in the conduction band are filled.

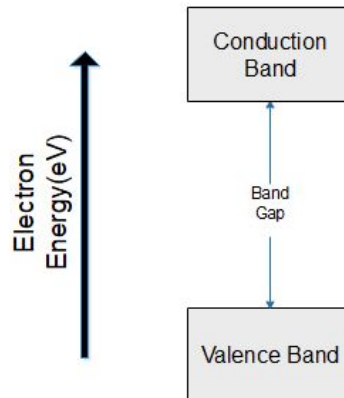


Figure 2.3: The valence band contains electrons in the outermost orbital of an atom. When the electrons are excited they jump from the valence band to the conduction band. The bandgap separates these two bands measured by energy in units of electron volts

The electrons need energy to make the jump between the two bands as seen in figure 2.3. One method is exciting the electrons by sending light to the semiconductor. This energy measured in electron volts(eV) increases as you jump from the valence to the conduction band. Similarly in order to drop from the conduction to the valence band there would need to be a release in energy. In certain cases this energy comes off as photons of light.

2.3 Interference Fringes: Destructive and Constructive Waves

As light interacts with a new medium, the wave will either reflect off the medium’s boundary or transmit through. The amount of light flux transmitted over the incident flux determines the transmittance. The reflectance is the same except the ratio of the reflected lights flux and incident light is taken. In figure 4, the incident electric field(E_{0i}) at some angle to the interference. After interacting with the first layer of TiO_2 , the reflected light will experience a π phase shift due to interacting with a medium of higher index of refraction.

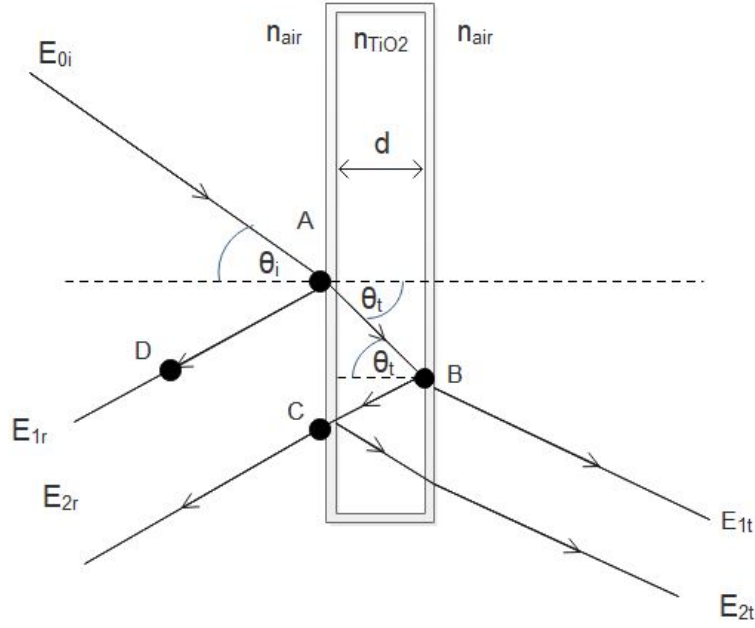


Figure 2.4: Looking at light as a electric field and magnetic field, the electric field is in normal to the plane of incidence. After interacting with the first interface,a portion of light reflects, some transmits through and into the TiO₂. The light inside reflects and transmits until all the light either absorbed from the bandgap, transmits or reflects.

Due to the phase shift the reflected light,there will be optical length difference(OPD. In equation 7, the OPD is represented using the thin film seen in figure 2.4 for the first reflected light wave.

$$\Lambda = n_{TiO_2}(AB + BC) - (AD)n_{air}, \quad (8)$$

Expanding this to an m number of orders, will result in equations 9 and 10. One where the two waves interfere constructively seen in equation 9 and one where they destructive interfere seen in equation 10

c

$$2n_{TiO_2}d\cos(\theta_t) = (m + \frac{1}{2})\lambda_0, \quad (9)$$

$$2n_{TiO_2}d\cos(\theta_t) = (m)\lambda_0, \quad (10)$$

In experimental work these interference patterns will appear as fringes in the reflectance and transmittance data. The fringes with a maximum of reflectance will infer a minimum in the transmittance and visa versa. This detail will important for analyzing the transmission and reflection data.

3 Materials and Methods

3.1 Grating Spectrometer

The in house grating spectrometer Dr.McIntyre's lab measures the transmission and reflection of incident light after passing through thin films. The spectrometer requires a xenon lamp light source powered by a LPS 251 Lamp Power Supply. An ozone eater is attached to the rear of the lamp to prevent ozone from leaking into the nearby environment caused by the ultraviolet radiation projected by the lamp. The light from the xenon lamp, contains wavelengths from 185 nm to 2000 nm[10]. Realigning

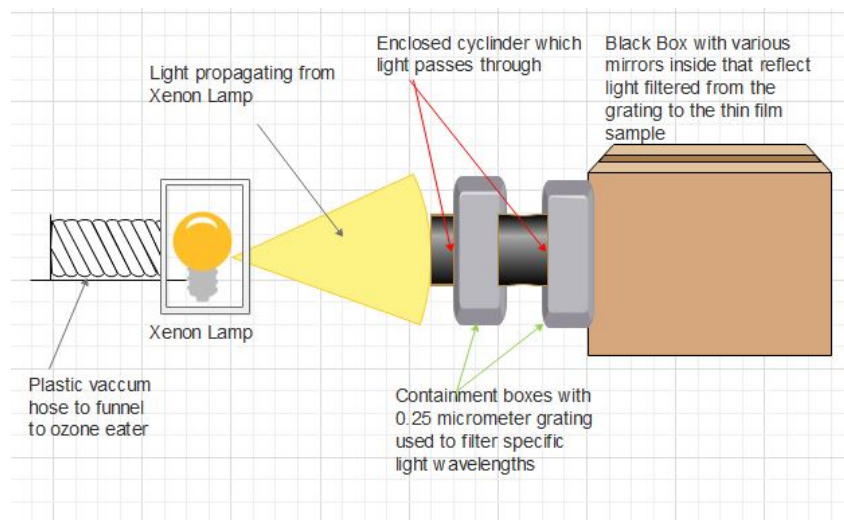


Figure 3.1: Grating Spectrometer setup with a xenon lamp producing a spectrum of light from 185 nm to 2000 nm. The light reflects from the diffraction grating in containment boxes, before entering a concealed box with optical lenses and a detector arranged for T and R spectroscopy

the grating angle to the incident light changes which wavelengths reflect from the gratings surface. The first containment seen in figure 3.1, will filter out wavelengths except for ones between 200 nm to 1000 nm while the second filters out the light again by 1 nm increments within the previously mentioned range. Light enters the black box through a 13.6mm opening and then gets magnified by a convex lens. A mirror redirects the light by 90 degrees in the counterclockwise direction. An iris is position afterwards to alter the amount of area the light passes through a circular opening. Thin films are placed in a stand and aligned with the light passing through the iris.

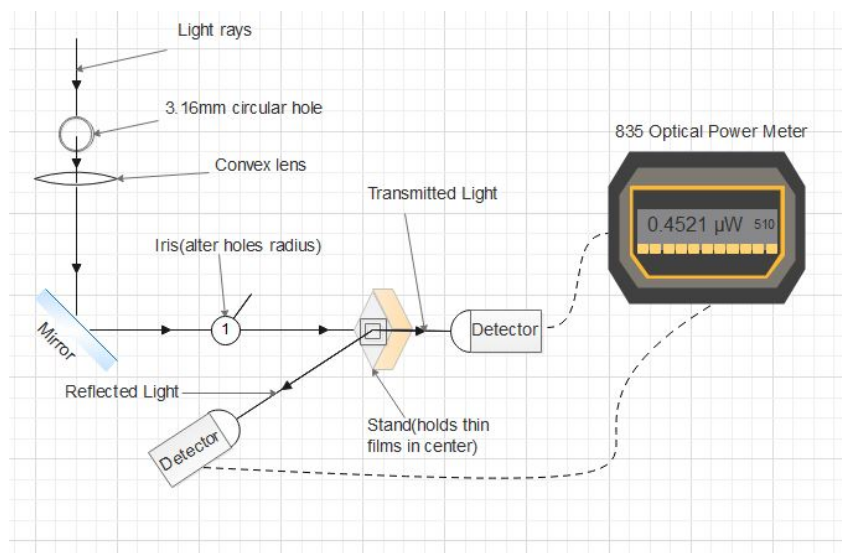


Figure 3.2: The incident light follows a selected path with a mirror reflecting all the light perpendicular. An iris is used to lessen the intensity to prevent overexposure to the detector. The data is recorded on an external optical power meter.

The transmission and reflection of light were recorded in units of voltage with the Si-detector. To properly quantify the data, the total voltage of light with no film was recorded before each T and R measurement. The absence of light was also recorded to correct for any scattering and residual photons or noise created by electromagnetic wave interference.

To utilize this light for T and R measurements, an optical power detector with a circular lens allows light to transmit through which then travels through a fiber optic cable to a 835 Optical Power Meter. This setup is seen in figure 3.2 where the power output was measured in terms of watts. This detector has two positions, one for the transmission and one for the reflection of the thin films. To analyze this data, the proprietary software known as LabVIEW is used to store the transmission and reflection data. Graphs are plotted with this data in LabVIEW and also exported into an Excel notebook known as Index Calc

3.2 Error due to alignment

The majority of the spectrometer's orientation remains fixed, however with each new film the light reflected will produce a different reflection angle. The transmission is unaffected continuing along the same path as the incident light. To account for this angle difference in each film, the stand holding the TiO_2 can be rotated horizontally and vertically. Aligning the reflected light with the detector properly is imperative for consistent and accurate results.

3.3 Index Calc

The transmission and reflection data collected from LabVIEW can be imported into a excel notebook written by Levi Kilcher and modified by James Haggerty known as Index Calc. The main purpose of this notebook is to use the transmission and reflection data to determine the thickness and index of refraction for TiO_2 . The reflection graph displayed in Index Calc places the experimental data along with a fitting curve. This fitting curve is dictated by the fringes at different wavelengths as well as the thickness of the thin film. The fringe values are recorded into the notebook and a guess for the thickness are the preliminary values needed to approximate the fit. Two buttons control the first step of the fitting, first by using the fringes to find a reasonable thickness and second doing the reverse. Iterating over these two buttons over time produces a better fit to the experimental data.

3.4 Tauc Analysis

To determine the bandgap values, a process known as a Tauc analysis was performed[12]. Figure 3.3 presents an example of the plots produced from the analysis. The curves change as a function of energy in electron volts. For the direct bandgap the y axis value is $(\alpha E)^2$ and the indirect bandgap it is $(\alpha E)^{\frac{1}{2}}$. The linear behavior is seen close to the onset energy, this is where a linear fit is placed and extrapolated to the x axis. This is done to determine the onset absorption which will occur just before the linear increase.

The Urbach tail, which is the exponential portion of the curve to the left side of the linear absorption curve. This portion can occur due to localized states that mix into the bandgap. This establishes the reasoning for making the linear fit extrapolate before the exponential drop off which would provide a inaccurate bandgap value.

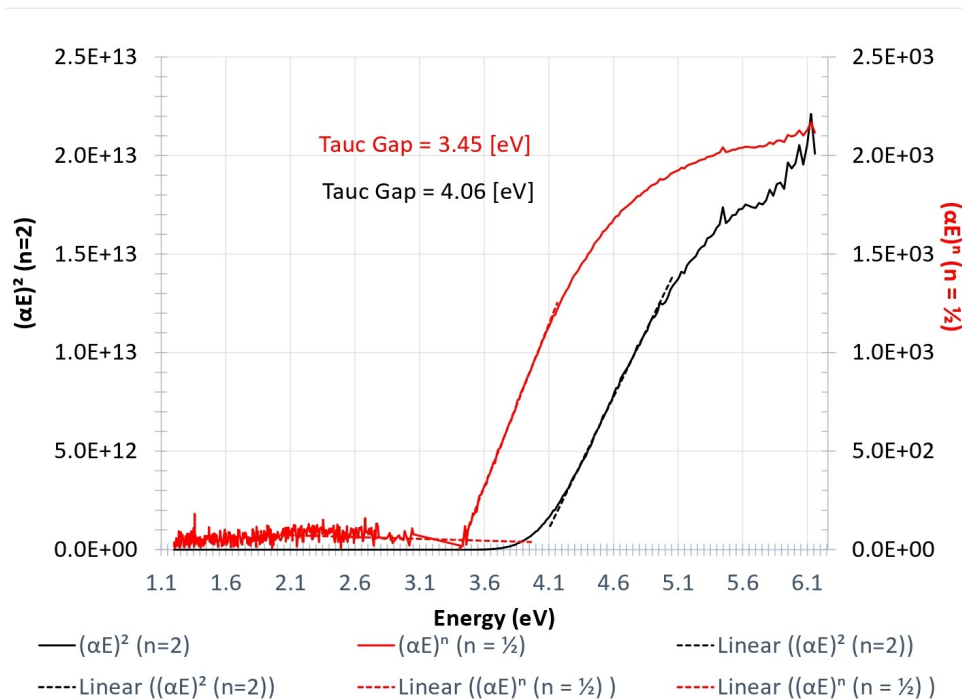


Figure 3.3: Tauc analysis for thin film sample TiO₂_085_Pre. The red curve represents the indirect bandgap and the direct bandgap is the black curve. The axes are colored appropriately to the curve colors. The bandgap energies are displayed in electron volts.

3.5 O₂ deficiency

Sample #	O ₂ (at %)	pO ₂
TiO2_S_065_Pre(rutile)	0.63	1.67
TiO2_S_065_Post(rutile)	0.65	1.67
TiO2_S_072_Pre(brookite)	0.64	2.86
TiO2_S_072_Post(brookite)	0.65	2.86
TiO2_S_085_Pre(anatase)	0.66	2.86
TiO2_S_085_Post(anatase)	0.65	2.86

Table 1: Oxygen gas content found for each pure phase polymorph thin film. There was a higher oxygen content found in anatase, brookite had slightly less and rutile was the least oxygen full. Blue indicates a brookite dominant polymorph thin film, green for anatase, and red for rutile.

Using an electron probe micro-analyzer (EPMA), Okan Agirseven from the Tate lab was able to determine the oxygen percentage portion for the thin films. The particle pressures of oxygen for each polymorph are also listed for reference. Table 1 shows us that the O₂ was highest in the anatase pure

phase polymorph film. With a higher oxygen content, there are less electron holes to be filled up and absorbed.

4 Results and Discussion

Transmission and reflection measurements were recorded for 24 thin films of TiO₂ on a SiO₂ substrate, which includes the amorphous and crystalline forms. Using T and R, the film thickness, index of refraction at 633nm and the bandgap were all determined. The following plots and data will be labeled in colors, blue for brookite, red for rutile and green for anatase polymorphs.

Sample #	Minimization Parameters ($X^2[R]$, $X^2[T]$)	Film Thickness(nm)	n @ 633nm	Sellmeier error
050_Pre	0.22,0.31	43.9	2.43	0.25
051_Pre	0.9, 0.37	34.2	2.43	0.73
051_Post	0.01, 0.14	34.9	2.53	0.94
052_Pre	0.87, 0.92	25	2.45	0.25
052_Post	0.99, 0.64	23.1	2.68	0.90
053_Pre	0.48, 0.40	26	2.08	0.30
053_Post	0.62, 0.52	28.95	2.22	0.09
054_Pre	0.83, 0.96	26	2.19	0.56
054_Post	1.95, 2.21	29.9	2.01	0.67
060_Pre	0.81, 0.46	20	2.64	0.67
060_Post	1.4, 0.78	21	2.6	0.47
065_Pre	0.95, 0.15	45.0	2.36	0.18
065_Post	1.2, 0.73	40.2	2.35	0.75
068_Pre	0.97, 0.50	55.1	2.46	0.34
068_Post	0.8, 0.46	25.0	2.38	0.39
072_Pre	0.4, 0.75	27.0	2.6	0.51
074_Pre	0.53, 0.30	54.9	2.37	0.63
074_Post	0.98, 0.44	55.1	2.45	0.98
077_Pre	0.84, 0.34	128.1	2.47	0.34
077_Post	0.88, 0.37	127.0	2.53	0.22
085_Pre	0.25, 0.24	38.0	2.53	0.75
085_Post	0.86, 0.29	38.0	2.54	0.89
086_Pre	0.69, 0.16	165.1	2.46	0.07
086_Post	0.85, 0.28	164.7	2.51	0.34

Table 2: List of all the thin films measured for their transmission and reflection. The refractive index at 633nm and thickness come from the index calc excel sheet analysis. The minimization parameter and Sellmeier error were used to quantify the error of the reflection and transmission fits for determining the optical properties.

Table 2 is the list of TiO₂ pre and post anneal thin films, each had transmission and reflection measurements recorded over the wavelength range 200-1000 nm. The minimization parameters provide a value to indict the amount of error when fitting to the transmission and reflection data. Values less than 1 provide the best fit, between 1 and 2 is considered a good fit, and values over 2 indicate a bad fit. The thicknesses varied on accuracy based on these minimization parameters. The refractive indices were found from altering the Sellmeier coefficients that makes up the Sellmeier equation. A similar minimization parameter was recorded for the Sellmeier coefficients fitting the index of refraction curve depicted by the fringe data input into Idex Calc. The thickness and refractive indices were compared with ellipsometry data found by the Tate Lab from Joseph Kreb, which can be found in the appendix.

4.1 Transmission and Reflection

The calculated transmission and reflection measurements produced graphs as seen in figure 4.1 with sample TiO₂_086_Pre. The expected corrected transmission should follow equation 6 where the light exists in transmission, reflection or absorbance. This follows the law of energy conservation, where all the energy before interacting with the system must be retained in the thin film through one of these three behaviors. For sample 86_Pre, between 200-320nm, around 30% of intensity from the reflection, 0% from transmission, indicating the remaining portion of light is absorbed. This area of high absorption is where the bandgap exists. After this region, the reflection of light and transmission are much higher with the absorption values dropping significantly as the wavelength increases to 1000nm. From Eqn 6, $\frac{T}{1-R}$ hovers at 90% of the raw intensity of light. Therefore we can conclude that a portion of the intensity is absorbed however it is not due to the bandgap. One possible reason is the defect states present could produce an absorption outside the bandgap.

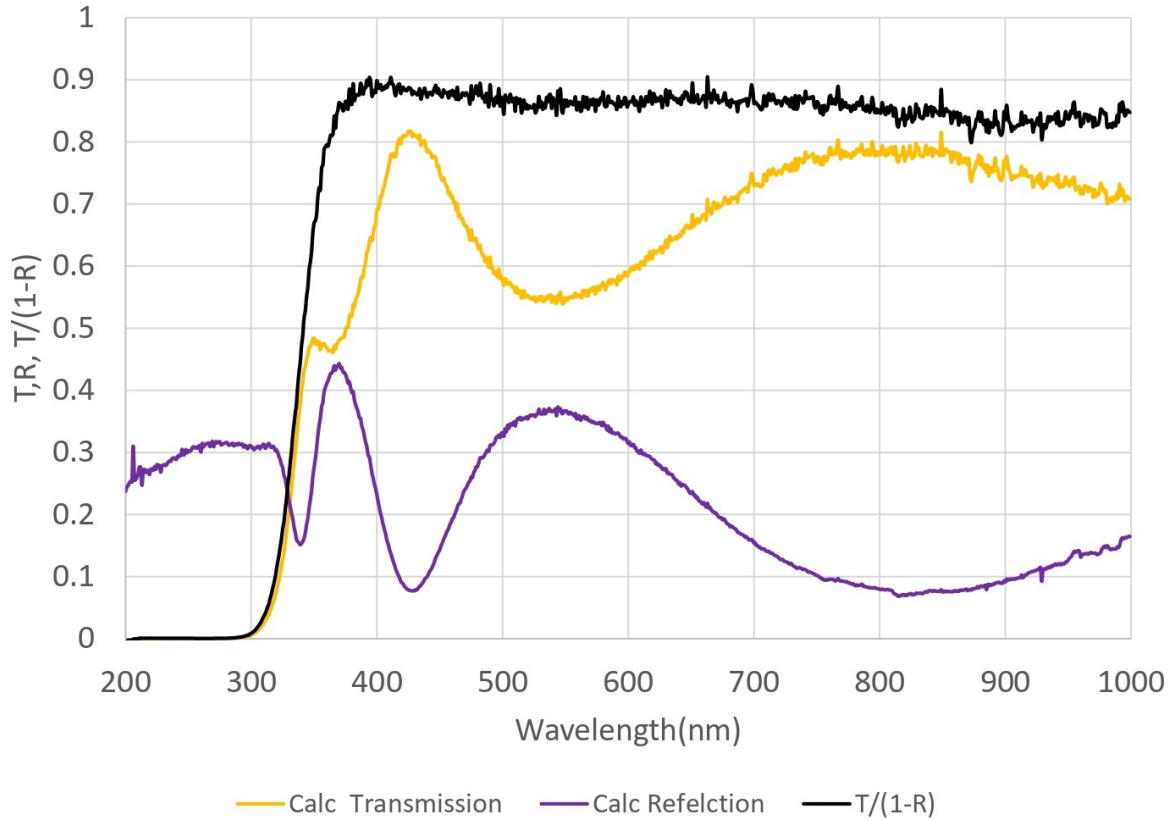


Figure 4.1: Transmission, reflection and $\frac{T}{1-R}$ for a pre annealed anatase thin film. From $\frac{T}{1-R}$ we can see around 90% of light is absorbed after the bandgap absorption(300 nm - 400 nm). The y axis scales by the ratio of light from incident to the reflected or transmitted. This does not present the actual value of transmission recorded during this experiment.

The SiO₂ 1mm substrates were used due the samples low absorbance across the UV-VIS-NIR spectrum. Looking at figure 4.2, the transmission hovers at 92% from 220nm to 1000nm and the reflection contains the other 8% of light. Some noise appears between 200-220nm in the SiO₂ intensity plot. The intensity exceeding 100% indicates a misalignment of the incident beam. If there was some absorption within this region, that would carry over to the TiO₂'s intensity plot seen in figure 7. So we can conclude that the SiO₂ substrate has a negligible effect on the absorption seen within the UV-VIS-NIR spectrum.

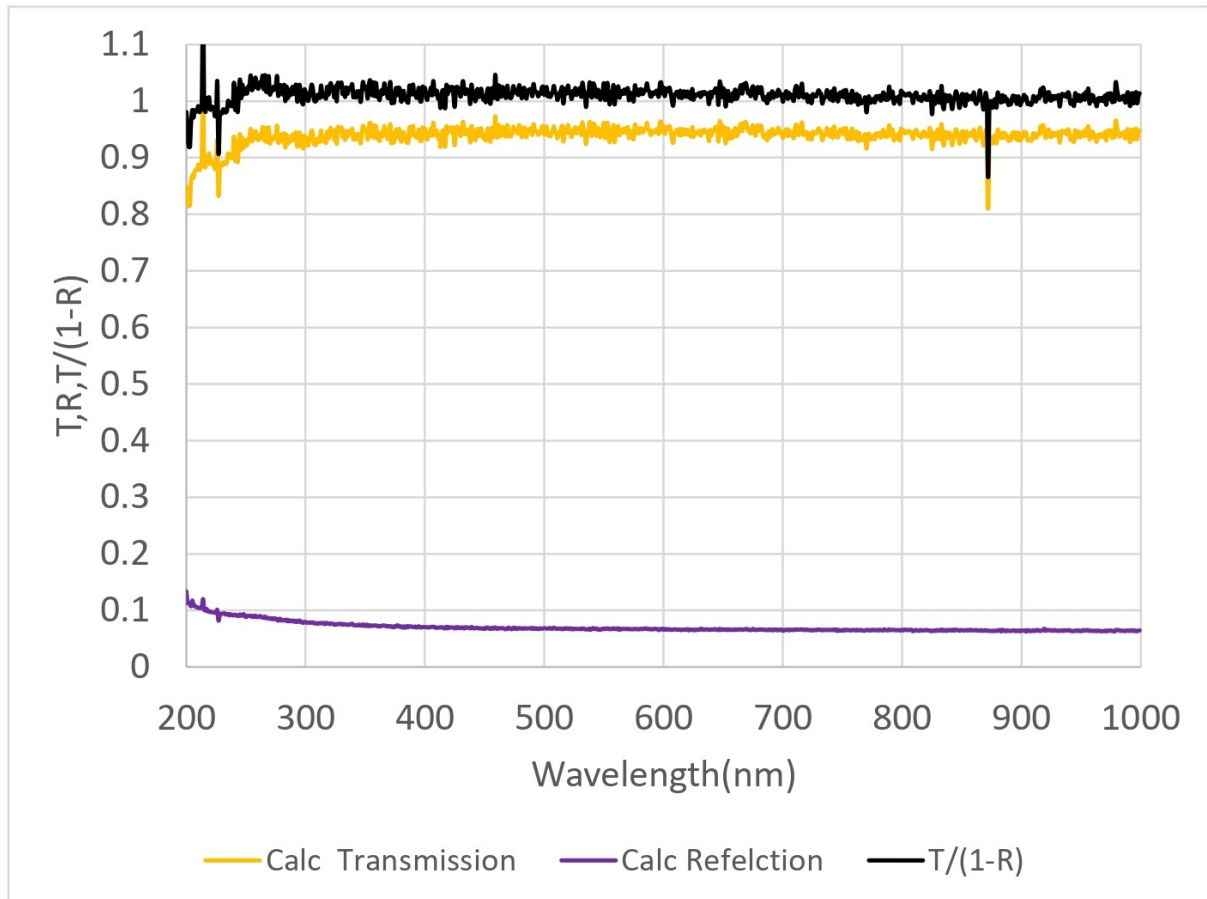


Figure 4.2: Transmission, reflection and $\frac{T}{1-R}$ for 1mm SiO₂ substrates. These pieces of glass transmits almost all light between 200-1000nm. There around 10% of light on average in this range reflected. Nearly 0% of light is absorbed, indicating the bandgap does not absorb light in this wavelength region.

Now that both the transmission and reflection behavior for the substrates and thin films are established, we want to try and find some distinction between the films. The thickness, atomic arrangement, and amorphous precursors are three physical properties that directly affect the optical properties. A method for analyzing these affects is plotting the pre and post anneal $\frac{T}{1-R}$. These plots can be seen in figure 4.3 and 4.4, where the rutile, brookite, and anatase are indicted as mentioned previously by their distinct color choice. In figure 4.3, we see the $\frac{T}{1-R}$ curves with the only noisy data in the rutile curve in the wavelength region 800-1000 nm's. There is a clear trend of rutile thin films transmitting less than brookite and anatase in the 350-1000 nm wavelength range. Brookite transmits better than the rutile thin film and anatase overall has the best transmission in this range.

After annealing the structure of the TiO₂ becomes highly ordered. In the post anneal seen in figure 4.4, we see the brookite thin films increase in transmission in between 350-1000 nm, going from around 95% up by about 3 to 5%. The only film which still observes a high absorption in this range is the rutile

one. In table 1 we observed the O₂ content increase for brookite and rutile films when transitioning from amorphous to crystalline. The anatase films decrease in oxygen content, which at this moment we don't have an explanation for.

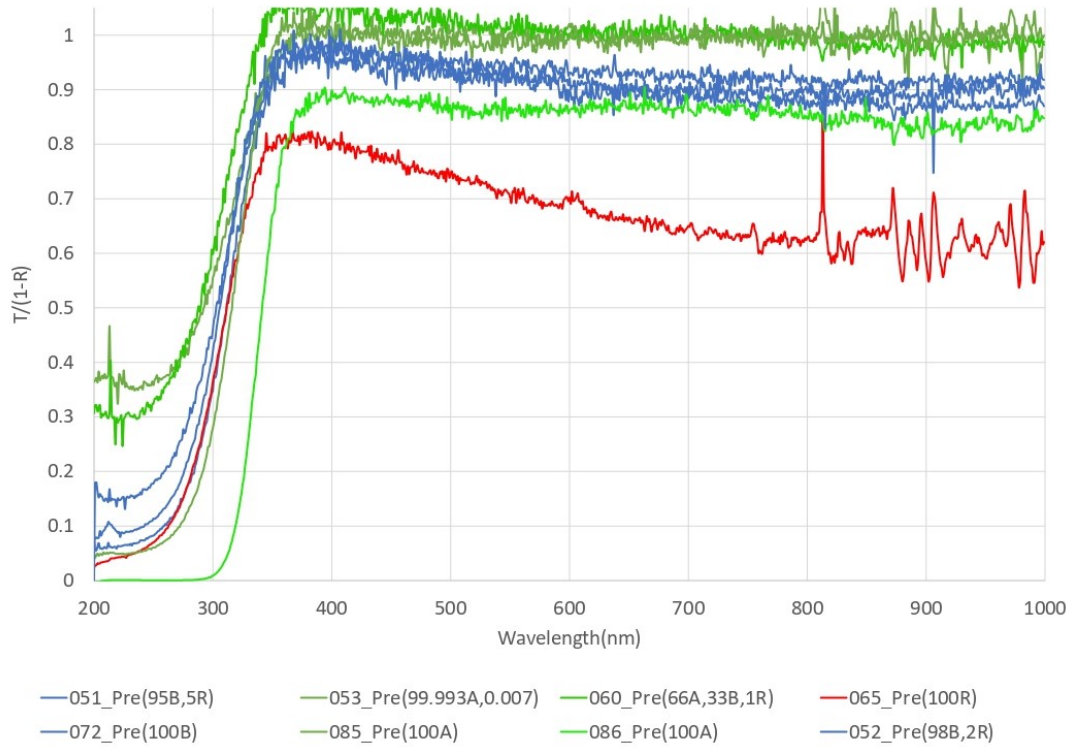


Figure 4.3: $\frac{T}{1-R}$ curves for a select set of pre anneal amorphous precursors taken from table 2. The same color arrangement for the dominant polymorphs of each thin film is used. From 250 nm to 380 nm the bandgap absorbance is seen with anatase films having higher transmissions on average during this region. In the longer wavelength region (> 600 nm), the transmission of rutile and brookite decrease while anatase remains nearly 100% transmission.

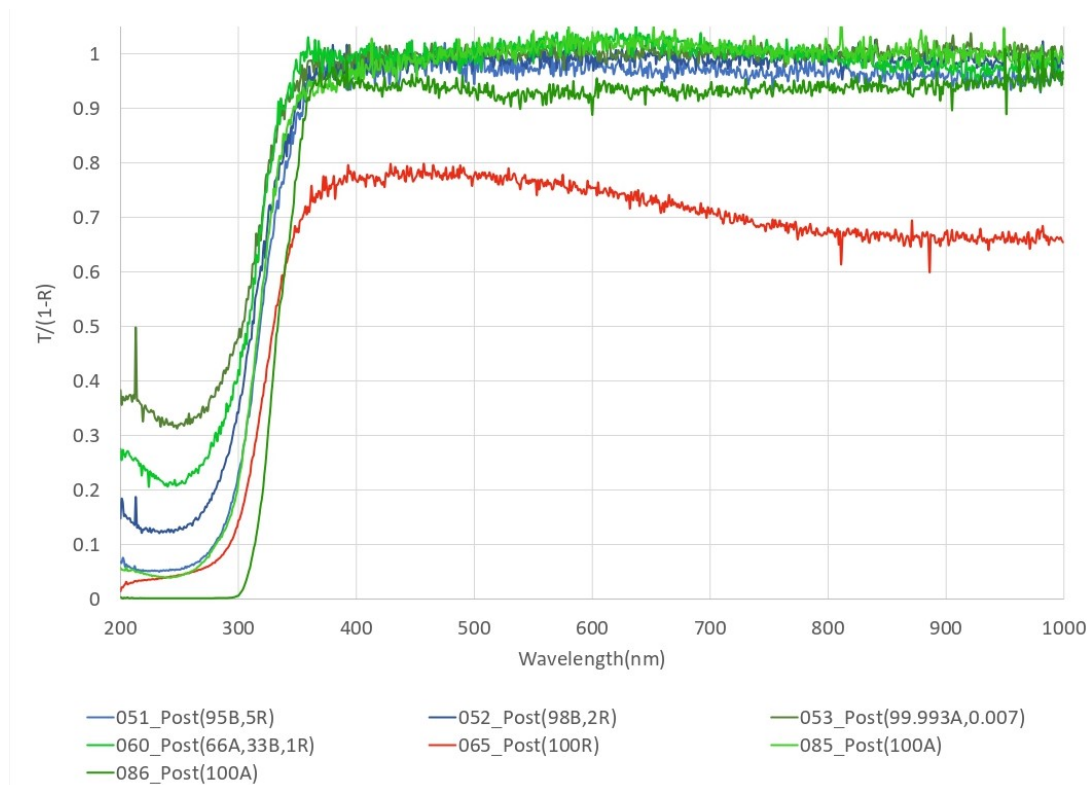


Figure 4.4: $\frac{T}{1-R}$ curves for a select set of post anneal crystalline films taken from table 2. There is a increase transmission for the rutile and brookite polymorphs compared to the curves for the amorphous precursors. Brookite experienced the highest increase, transmitting close to 95% in the long wavelength region. The anatase dominant polymorphs remain mostly unchanged in transmission in the longer wavelengths.

The correlation however between brookite and rutile growing in transmission as well as O_2 content seems to hold as a possible reason for the absorption observed in the 350-1000 nm range. The crystalline films become more oxygen full therefore this causes a decrease in absorbance and a increase in transmission.

4.2 Absorption Coefficient

In figure 4.5 and 4.6, we see the respective absorption coefficient values as a function of the wavelength calculated with equation 7. We can more clearly distinguish the absorbance of each thin film. Anatase has values of absorbance coefficients ranging from 0 to $10,000 \text{ cm}^{-1}$. There is one sample, 60.Pre which most likely was not properly aligned during the experiment causing unrealistic behavior of a negative coefficient number. The pre anneal brookite thin films resided much higher between $10,000$ to $40,000 \text{ cm}^{-1}$. Rutile values were the highest go from $40,000 \text{ cm}^{-1}$ up to $110,000 \text{ cm}^{-1}$. These films were determined to be at a variety of thickness measurements however there are clear sections defined

for each polymorph. This indicates that the coefficients regardless of thickness are restricted to specific values, only scaling up or down within this region by their thickness.

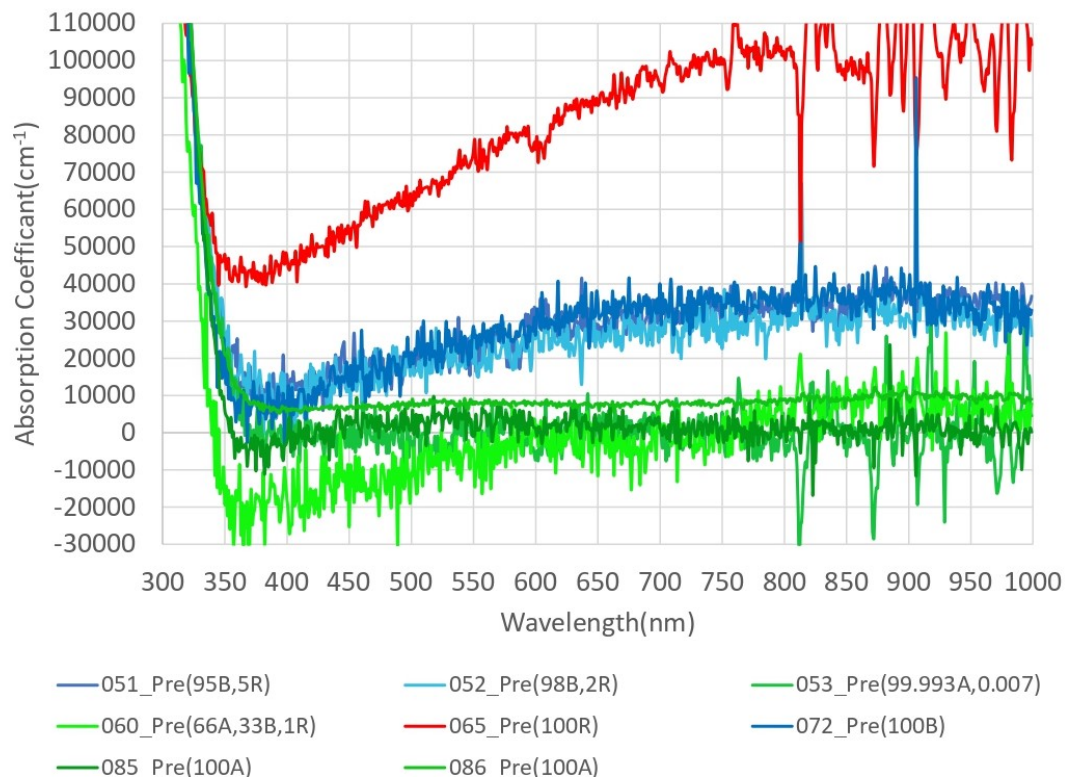


Figure 4.5: Absorption coefficient vs wavelength curves for the pre anneal amorphous precursors. This provides evidence of the absorption seen in the $\frac{T}{1-R}$ figure 4.3. Rutile has the highest absorption coefficient, brookite around 5 times less on this scale. Anatase from 350 nm to 1000 nm absorbed nearly 100% with some noise after the bandgap absorption (350 nm) producing negative coefficients which are not realistic.

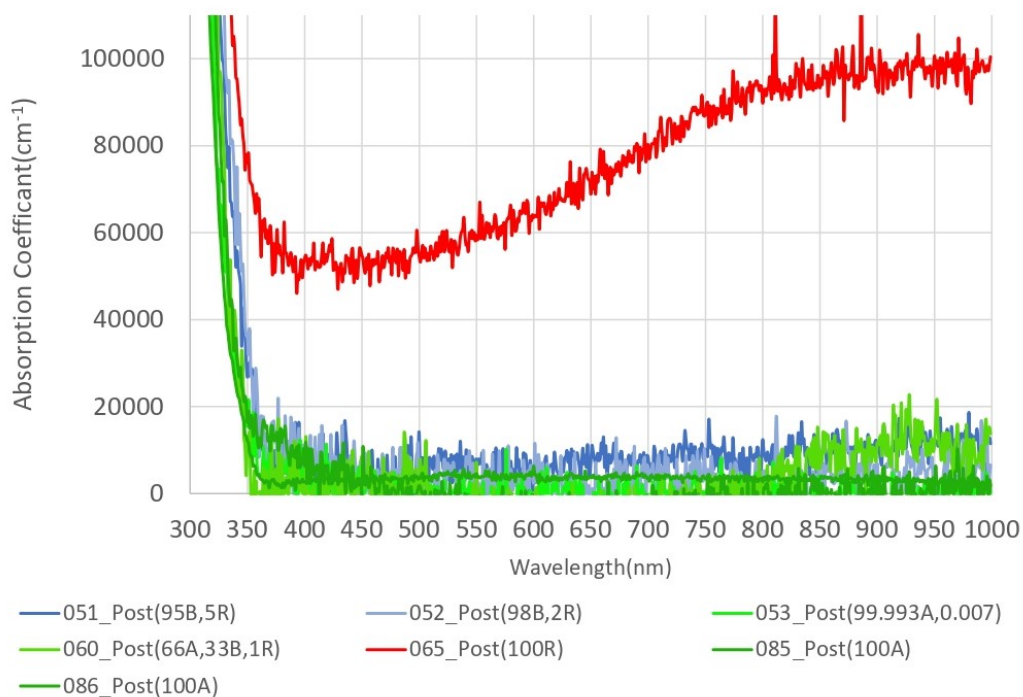


Figure 4.6: Absorption coefficient vs wavelength for crystalline polymorphs. The absorption seen in figure 4.4 is shown to be still high for the rutile polymorph. Brookite and anatase contain the lowest absorption coefficients across the 350 to 1000 nm wavelengths.

4.3 Pure Phase Films

All the $\frac{T}{(1-R)}$ curves shown so far are from thin films with various thicknesses and phase fraction percentages. Samples 65, 72, and 85 were all produced with 100% phase of each polymorph. These curves in figure 4.7, were plotted with both pre and post anneal thin films of TiO₂. For sample 65, which was 100% rutile, the thickness measurements were 45nm for the pre and 40.2 for the post. The anatase sample was 85, which for pre and post were both essentially 38nm. Due to the current situation with the pandemic, sample 72 pre was only measured with no comparison to the post for this analysis. With the brookite and anatase thin films isolated around the same value thickness, the effects of the thickness should be negligible to the curves. In this figure, it is more clear that rutile tends to absorb around the 60-70% range for wavelengths 800-1000 nm. The anatase films were clearly the least absorbent as expected with transmissions around 100% recorded for wavelengths 400-1000 nm. These plot show that when considering thickness independence, the phase each polymorph is made of will affect the absorbance seen between 400-1000 nm.

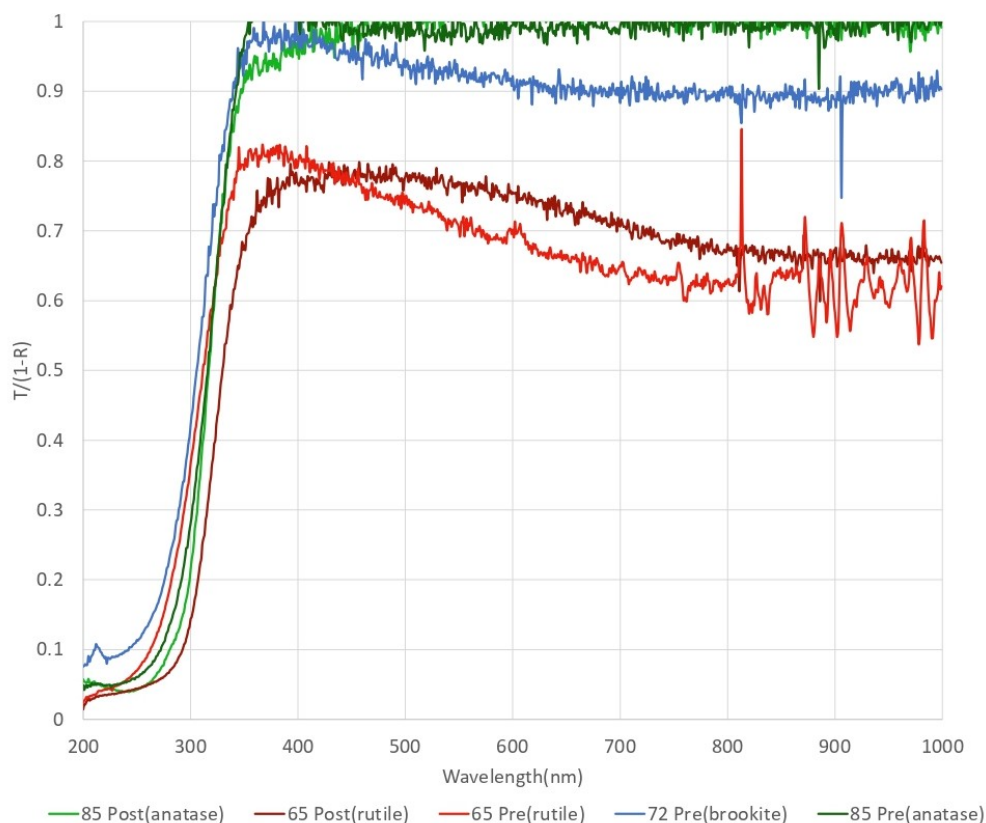


Figure 4.7: $\frac{T}{1-R}$ plots for samples 85 pre and post, 72 pre, and 65 pre and post. The expected trend is that anatase transmits or reflects nearly 100% of light at wavelengths beyond the bandgap range(250-350) followed by a slightly absorbent brookite than finally rutile absorbing the most past this. This also helps further display the effects of O₂ deficiency on the absorbance seen outside of the bandgap.

4.4 Band Gap Analysis

A Tauc analysis was performed for each thin film to find the indirect and direct bandgap values. The goal was to formulate any unique behavior that occurred with the films. In table 3, the calculated values for each thin film, were found for all 24 samples. Initially the behavior seen was a decrease in the bandgap energy was observed for the indirect and direct. Certain thin films however experienced a significant increase in energy after the annealing process. Only one direct bandgap thin film, 86, increased from 3.9 eV to 4 eV. The indirect bandgap values were a mixture of increasing, decreasing, and remaining the same. There was not clear distinction, unlike the direct bandgap with a clear decrease on nearly all the thin films.

Sample 86 was the thickest film at 165.1 nm pre anneal, sample 77 however was also relatively thick compared to the other films at 128.1 nm in the amorphous state and did not experience the same increase. The other corresponding 100% anatase phase samples to 86, all decreased in energy after

the annealing process. There was not any discernible property for samples which increased in energy and those that decreased. None of the unique properties appeared to play a role including the thickness and crystalline phase composition.

Sample ID #	Direct Bandgap(eV)	Indirect Bandgap(eV)
050_Pre(95A,5B)	4.1	3.4
051_Pre(95B,5R)	4.1	3.5
051_Post(95B,5R)	4	3.6
052_Pre(98B,2R)	4.1	3.5
052_Post(98B,2R)	4.0	3.4
053_Pre(99.993A,0.007)	3.9	3.3
053_Post(99.993A,0.007)	3.8	3.4
054_Pre(96B,4A)	4.1	3.6
054_Post(96B,4A)	3.8	3.5
060_Pre(66A,33B,1R)	4.0	3.5
060_Post(66A,33B,1R)	3.9	3.5
065_Pre(100R)	4.2	3.6
065_Post(100R)	3.9	3.6
068_Pre(100A)	4.0	3.4
068_Post(100A)	3.9	3.5
072_Pre(100B)	4.1	3.6
074_Pre(90.5B,9.5R)	4.2	3.4
074_Post(90.5B,9.5R)	4.0	3.4
077_Pre(63B,37R)	4.1	3.5
077_Post(63B,37R)	4.0	3.5
085_Pre(100A)	4.1	3.5
085_Post(100A)	4.0	3.4
086_Pre(100A)	3.9	3.4
086_Post(100A)	4.0	3.4

Table 3: Direct and indirect bandgap results in terms of electron volts(eV). While a polymorph can only possess either a direct or indirect bandgap, both were calculated as the mathematical process does not provide which bandgap the thin film has.

Phase and Anneal State	Direct Bandgap(eV)	Indirect Bandgap(eV)
Anatase-Pre	4.0	3.4
Anatase-Post	3.9	3.4
Brookite-Pre	4.1	3.5
Brookite-Post	4.0	3.5

Table 4: Average values for the direct and indirect bandgaps for the amorphous precursors and the polymorphs. Anatase and brookite experienced a decrease in direct bandgap energy when transitioning from the amorphous structure to crystalline. The indirect bandgaps remained fixed between the pre and post annealed thin films.

In table 4, there are the average bandgap values determined for the anatase and brookite thin films. Rutile was not considered as there was only one thin film, so a average would be nonsensical. The pre annealed state films on average produced higher direct bandgap values than the post annealed films. This behavior did not carry over to the indirect where the average was the same for pre to post for both sets of films. There is not any indication on why the small shift was present in the direct bandgap analysis and not the indirect. The change could be related to the defect states which were shown to be a possibly affecting the long wavelength regions however this is simply speculation. The presented data does not provide enough evidence to determine the cause for the possible decrease in energy found with the direct bandgap results.

5 Conclusion

The purpose of this research was to identify the optical properties of titanium dioxide. The process for depositing TiO_2 onto SiO_2 did not have a defined model for creating thin films with known amorphous precursors. With recent developments in the Tate lab, Okan Agirseven has developed a method for setting parameters to know the crystalline phase structures before the annealing process was performed on these films. By measuring the transmission(T) and reflection(R) using T and R spectroscopy, within the ultraviolet to near infrared range(UV-VIS-NIR), the thickness, absorption and refractive indices of the thin films were calculated. These T and R measurements were recorded for the sputtered amorphous precursors and the corresponding crystalline films.

In the research preceding this project, Patrick Berry from the Tate Lab performed similar T and R measurements for TiO_2 thin films of various thicknesses and crystalline state phases. He was not able to measure three pure phase polymorphs with the same thickness. With this project, similar thickness films of pure phase were produced and measured for their T and R. The absorption in the longer wavelength range($> 600 \text{ nm}$) observed was also seen in previous results analyzed by Berry for mainly brookite and rutile thin films. The current hypothesis is the oxygen deficiency create defect states that cause absorption in these long wavelengths. Results for $\frac{T}{1-R}$ indicate from pre to post anneal there is a decrease in absorption as more oxygen vacancies are filled. Oxygen deficiencies is a reasonable explanation, however analyzing more thin films of pure phases at higher thicknesses would provide a more concrete understanding of this behavior.

The bandgap was explored for amorphous precursors and their crystalline form. Anatase films on average had a lower bandgap energy for the amorphous films for the direct and indirect bandgap compared to the brookite films. The direct bandgaps decreased in energy from pre to post anneal for anatase and brookite. The indirect bandgaps for these two polymorphs experienced no decrease in energy from pre to post anneal. For the singular rutile pure phase thin films, the occurrence of the direct bandgap decreasing in energy and the indirect bandgap remaining unchanged. There was not a clear indication on why this occurred and further research will likely provide a clearer explanation of this behavior observed. Overall, the goal to determine if similar thickness pure phase films produced results seen in previous research was a success and is open for further developments to be explored.

References

- [1] Roy, P., Berger, S., and Schmuki, P. (2011). TiO₂ Nanotubes: Synthesis and Applications. *Angewandte Chemie*, 50(13), 2904–2939. <https://doi.org/10.1002/anie.201001374>
- [2] Park, J. Y. (2018). How titanium dioxide cleans itself. *Science (New York, N.Y.)*, 361(6404), 753–753. <https://doi.org/10.1126/science.aau6016>
- [3] Agirseven, O., Rivella, D. T., Haggerty, J. E. S., Berry, P. O., Diffendaffer, K., Patterson, A., Krebs, J., Mangum, J. S., Gorman, B. P., Perkins, J. D., Chen, B. R., Schelhas, L. T., and Tate, J. (2020). Crystallization of TiO₂ polymorphs from RF-sputtered, amorphous thin-film precursors. *AIP Advances*, 10(2), 025109. <https://doi.org/10.1063/1.5140368>
- [4] Berry, Patrick (2019). Characterizing Optical Signatures of TiO₂ Precursors[Unpublished bachelor's thesis]. Oregon State University.
- [5] Nair, Prabitha B., V. B. Justinictor, Georgi P. Daniel, K. Joy, V. Ramakrishnan, and P. V. Thomas. "Effect of RF Power and Sputtering Pressure on the Structural and Optical Properties of TiO₂ Thin Films Prepared by RF Magnetron Sputtering." *Applied Surface Science* 257.24 (2011): 10869-10875. Web.
- [6] Haggerty, J. E. S., Schelhas, L. T., Kitchaev, D. A., Mangum, J. S., Garten, L. M., Sun, W., Stone, K. H., Perkins, J. D., Toney, M. F., Ceder, G., Ginley, D. S., Gorman, B. P., & Tate, J. (2017). High-fraction brookite films from amorphous precursors. *Scientific Reports*, 7(1), 15232. <https://doi.org/10.1038/s41598-017-15364-y>
- [7] Hecht, Eugene. *Optics*. 3rd ed., Addison-Wesley, 1998
- [8] 2019. Diffraction Grating Physics. Retrieved from <https://www.newport.com/f/plane-ruled-reflection-gratings>
- [9] Y. Hishikawa, N. Nakamura, S. Tsuda, S. Nakano, Y. Kishi, and Y. Kuwano, *Jpn. J. Appl. Phys.*, Part 1 30, 1008 (1991). <https://doi.org/10.1143/jjap.30.1008>

-
- [10] Iguchi, T., Patel, S., Lares, M., & Hamamatsu Corp. (2010, October 8). A Guide to Selecting Lamps. Retrieved January 3, 2020, from https://www.photonics.com/Articles/A_Guide_to_Selecting_Lamps/a44487.
- [11] Casiday, Rachel, and Regina Frey. "Bonds, Bands, and Doping:" Bonds, Bands, and Doping: How Do LEDs Work?, June 2007, www.chemistry.wustl.edu/edudev/LabTutorials/CourseTutorials/bb/LED/151_T2_07_LED.pdf.
- [12] Tauc, J., R. Grigorovici, and A. Vancu. "Optical Properties and Electronic Structure of Amorphous Germanium." *Physica Status Solidi (b)* 15.2 (1966): 627-37. Web.

6 Appendix

6.1 Section 1: Ellipsometer vs Spectrometer Comparison

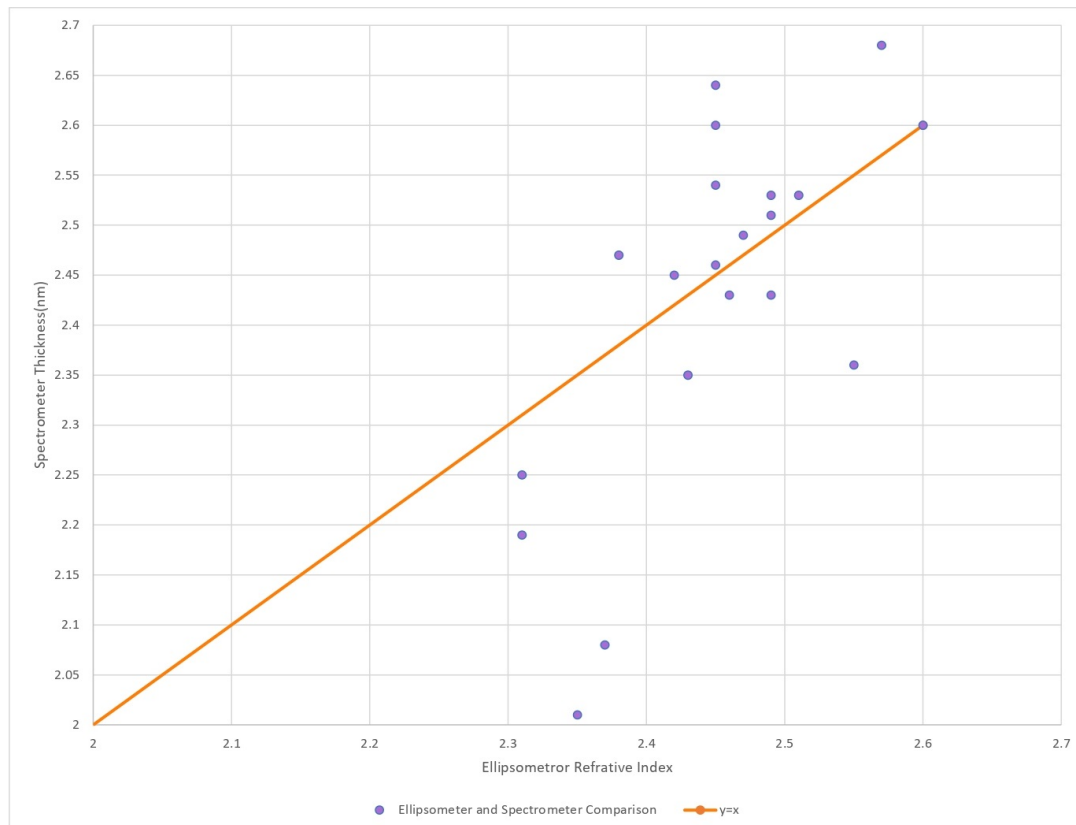


Figure 6.1: Comparison between ellipsometer and spectrometer thickness values. The ellipsometer values were provided by Joseph Kreb from the Tate Lab.

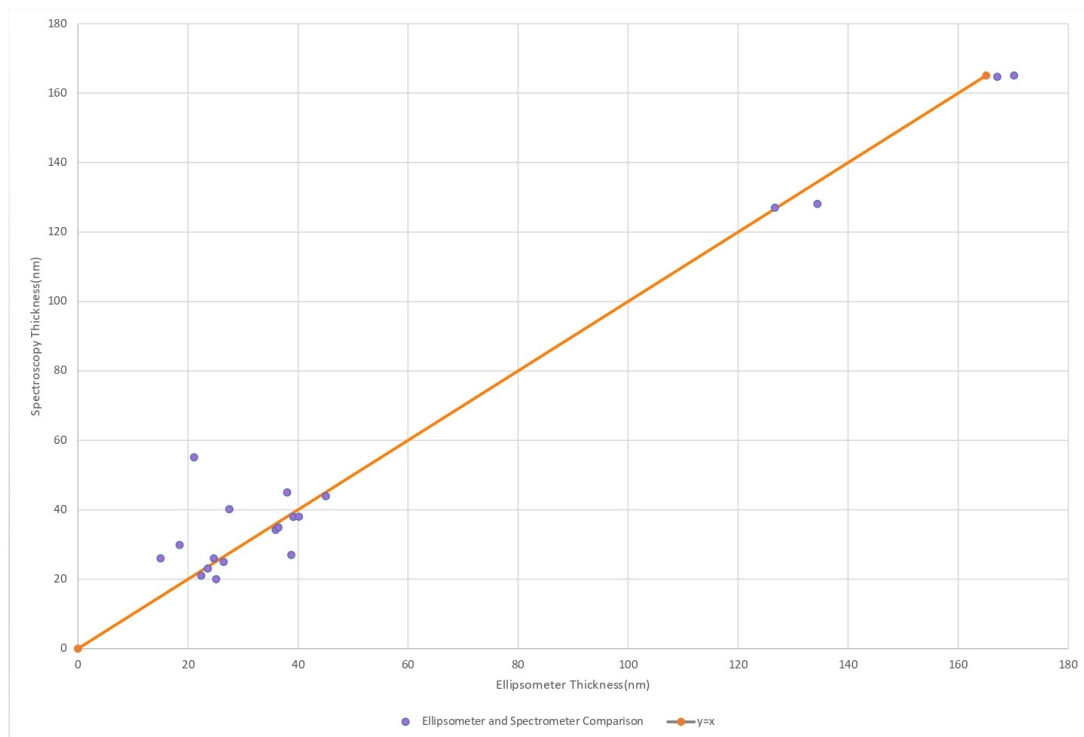


Figure 6.2: Comparison between ellipsometer and spectrometer refractive index values at 633 nm. The ellipsometer values were provided by Joseph Kreb from the Tate Lab.